Diffusion Monte Carlo and PIMD Calculations of Radial Distribution Functions Using An Updated CCSD(T) Potential for CH_5^+

Chen Qu,[*,†] Qi Yu,[*,‡] Paul L. Houston,[*,¶] Priyanka Pandey,[‡] Riccardo Conte,[§] Apurba Nandi,[‡] and Joel M. Bowman[*,‡]

†*Independent Researcher, Toronto, M9B 0E3, Canada*

‡*Department of Chemistry and Cherry L. Emerson Center for Scientific Computation, Emory University, Atlanta, Georgia 30322, U.S.A.*

¶*Department of Chemistry and Chemical Biology, Cornell University, Ithaca, New York 14853, U.S.A. and Department of Chemistry and Biochemistry, Georgia Institute of Technology, Atlanta, Georgia 30332, U.S.A*

§*Dipartimento di Chimica, Università degli Studi di Milano, via Golgi 19, 20133 Milano, Italy*

E-mail: szquchen@gmail.com; qyu28@emory.edu; plh2@cornell.edu; jmbowma@emory.edu

Abstract

We report a new permutationally invariant polynomial (PIP) fit to CCSD(T)/aug-cc-pVTZ energies for CH_5^+ that provides fast analytical forces, unlike the original PIP fit of 2006. The new fit, which is slightly more precise than the previous one, is used in classical molecular dynamics, diffusion Monte Carlo and path integral molecular dynamics calculations of CH and HH radial distribution functions (RDFs) at temperatures of 10 and 50 K. Corresponding RDFs are also reported for $CD_3H_2^+$. The well-known quantum localization of the H atoms to the diatomic site from previous and present DMC calculations is maintained at 10 K but shows additional delocalization to the "CH_3^+" site at 50 K.

Introduction

Takeshi Oka, who reported a line list spectrum of CH_5^+ in 1999[1] and basically characterized it as unassignable, concluded 16 years later that this notoriously fluxional cation still earned the moniker "Enfant Terrible".[2] This all stems from the hyperfluxional nature of the nuclear motion of this Olah superacid.[3]

Early high-level electronic studies of this cation located very small saddle point barriers separating equivalent minima (of which there are 5!).[4,5] Pioneering direct, DFT path integral molecular dynamics (PIMD) calculations of the radial distribution functions were reported at 5 K.[6] It was concluded that the "...H_2 moiety, as well as the preservation of the general shape of the distribution, already suggest that CH_5^+ may still have a relatively well defined ground-state structure." The first global potential and dipole moment surfaces were reported in 2003 using a fit to thousands of MP2 electronic energies. The fit was done with permutationally invariant polynomials (PIPs) that are invariant with respect to all 120 permutations.[7] Diffusion Monte Carlo calculations of the ground vibrational state wavefunction using this PES were reported soon thereafter.[8,9] A modified Shepard interpolated potential based on CCSD(T)/aug-cc-pVTZ energies and DMC calculation of the ground vibrational state were reported in 2005.[10] In 2006 Jin *et al.* reported a global PES that dissociates to $CH_3^+ + H_2$.[11] The PES was fit to 36173 CCSD(T)/aug-cc-pVTZ energies and used PIP bases. The rms fitting error is 78 cm^{-1} for energies up to 30 000 cm^{-1} relative to the global minimum.

This PES has been used in numerous studies ranging from classical,[8,12] diffusion Monte Carlo[8,13] to a variety of quantum calculations.[14–19] However, a shortcoming of this fit is that it does not provide analytical gradients. While this did not hamper molecular dynamics calculations (which used numerical gradients) or diffusion Monte Carlo and quantum calculations (which need energies only), both of which were done as noted below. These calculations did find very floppy motion for the ground vibrational state with all H atoms interchanging and very broad distributions of radial distribution functions.[8,13,20] However,

the remnant of a CH_3^+...H_2 structure was found. This is in qualitative accord with the earlier DFT direct-dynamics PIMD calculations.

An interesting question about how deteuration might affect the structure was addressed in DMC calculations for $CD_3H_2^+$. It was found that the H atoms predominantly prefer the diatomic site.[8] In contrast microcanonical classical molecular dynamics calculations at the quantum zero-point energy find no preference for the H and D atoms at the diatomic site. So clearly this is an example of quantum localization at 0 K.

In order to study the temperature dependence of this localization, PIMD calculations need to be done. However, the lack of analytical gradients for the earlier PES make such calculations very computationally intensive and so those were not done. We have made substantial progress in developing PIPs, and now the current software does supply analytical gradients as well as fast reverse differentiation.

Here this new fitting software has been used to re-fit the original data set of energies. The properties of the updated PES are presented, and the new PES is used in DMC and PIMD calculations, mainly for $CD_3H_2^+$.

Methods

Potential Energy Surface

To construct the new potential energy surface, we explored three possible bases, all of "51" permutational symmetry in our notation (where all five H atoms permute) and with maximum polynomial orders of 5, 6, or 7. For order 7, we used a dataset of 23 799 geometries and energies; this is original data set in ref. 11, which had been calculated at the CCSD(T)/aug-cc-pVTZ level. This fit used 2290 coefficients and obtained a root mean squared fitting error (rmse) of 32 cm^{-1}, which is lower than the original (2006) fitting of rmse = 78 cm^{-1}. The lower rmse is a direct result of using a larger fitting basis than used in 2006. With order 6 and the same 23 799 data set, the fit had an rmse of 87 cm^{-1}. With order 5, and a slightly

smaller dataset of 21574 energies (which has lower maximum energy that from the set original data set), we obtained a fit with an rmse of 145 cm^{-1}. The 6th order fit appeared to be a good compromise, so all further work was done with that, after routines for calculating both analytical gradients[21] and reverse ones[22,23] were added. The final 6th order fit has 849 polynomials and 14 029 monomials. We further applied the weighting procedure to the data set which weighted the data inversely with energy, weight$= 0.2/(0.2+\Delta E)$, where ΔE is the energy above the global minimum in hartrees. Using the 21 574 data set whose maximum energy is 25000 cm^{-1}, the new fit gives an rmse of 53 cm^{-1}, a weighted rmse of 41 cm^{-1}, a mean absolute error (MAE) of 32.4 cm^{-1}, and an R^2 of 0.999926. (This unweighted rmse is only 20 cm^{-1} larger than the one for the 7th order fit.) A correlation plot evaluating the fit is shown in Fig. 1. Finally, we note that this fit is used in the DMC, PIMD and MD calculations described next.

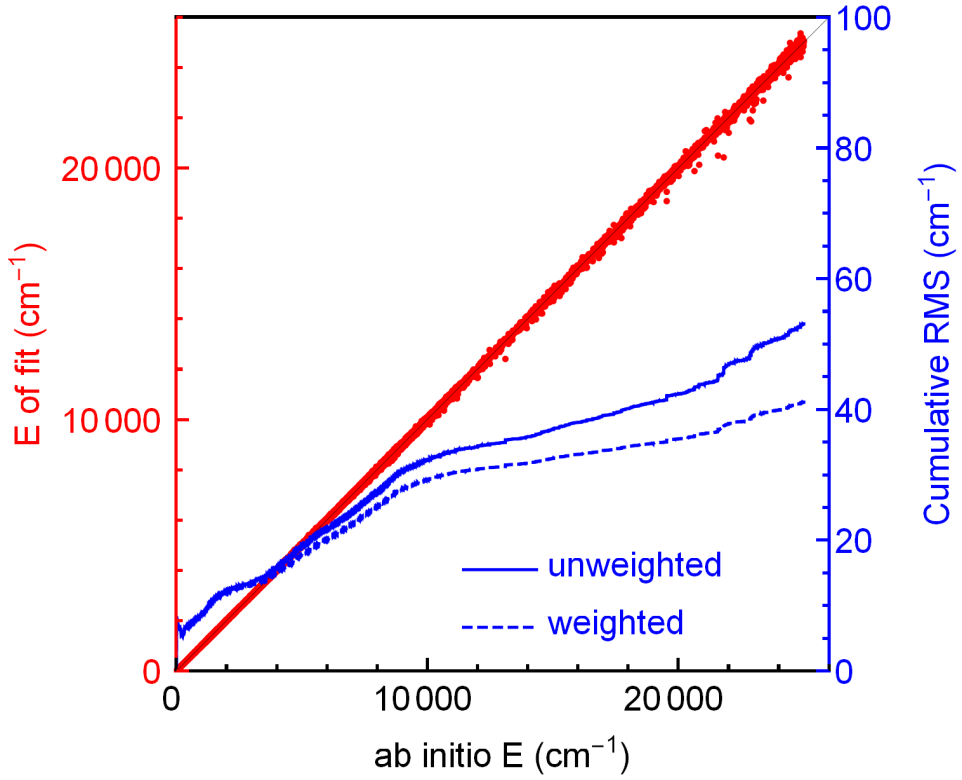

Figure 1: Correlation plot showing in red the energy of the fit versus the energy of the dataset. The blue curves and the right-hand axis give the rmse as a function of energy for both unweighted and weighted fitting.

Diffusion Monte Carlo

Standard unbiased diffusion Monte Carlo (DMC) calculations using in-house code were done to obtain the zero-point energy and wavefunction of CH_5^+ and the $CH_2D_3^+$ isotopologue using the new PES. The DMC method obtains the vibrational ground-state energy (i.e., zero-point energy) based on the similarity between the diffusion equation and the imaginary-time (denoted τ) Schrödinger equation with an energy shift E_{ref}

$$\frac{\partial\psi(\boldsymbol{x},\tau)}{\partial\tau} = \sum_{i=1}^{N} \frac{\hbar^2}{2m_i}\nabla_i^2\psi(\boldsymbol{x},\tau) - [V(\boldsymbol{x}) - E_{\text{ref}}]\,\psi(\boldsymbol{x},\tau) \tag{1}$$

The reference energy E_{ref} in the above equation is used to stabilize the diffusion system in its ground state and thus is the estimator of the zero-point energy.[24–26] We employed the unbiased, unconstrained implementation of DMC,[27] in which the DMC calculation starts from an initial guess of the ground-state wave function, represented by a population of $N(0)$ equally weighted Gaussian random walkers. These walkers then diffuse randomly in imaginary time according to a Gaussian distribution and the population is controlled by birth-death processes, given as

$$P_{\text{birth}} = \exp[-(E_i - E_{\text{ref}})\Delta\tau] - 1 \quad (\text{if } E_i < E_{\text{ref}}), \tag{2}$$

$$P_{\text{death}} = 1 - \exp[-(E_i - E_{\text{ref}})\Delta\tau] \quad (\text{if } E_i > E_{\text{ref}}), \tag{3}$$

where E_i is the energy of the ith walker. To maintain the number of random walkers at about the initial value $N(0)$, E_{ref} is adjusted at the end of each time step according to

$$E_{\text{ref}}(\tau) = \langle V(\tau)\rangle - \alpha\frac{N(\tau) - N(0)}{N(0)} \tag{4}$$

where $N(\tau)$ is the number of walkers at the (imaginary-)time step τ and $\langle V(\tau)\rangle$ represents the average potential energy of all of the walkers at that step. Finally, the average of $E_{\text{ref}}(\tau)$ over a sufficiently long period gives an estimate of the ZPE.

In this work, 5 DMC calculations were performed for $CH_2D_3^+$, and in each calculation, the imaginary time step $\Delta\tau = 5$ a.u. and $\alpha = 0.1$ are used. The random walkers are initiated at the global minimum, with the 2 hydrogens located in the "diatomic" site, shown in Fig. 2. In each DMC calculation, the number of walkers is 50 000, and these walkers are equilibrated for 5000 time steps followed by 100,000 propagation steps. The Cartesian coordinates of the walkers at the last step were recorded and their interatomic distances were analyzed.

Path Integral Molecular Dynamics

The Path Integral Molecular Dynamics (PIMD) method is a widely used method to obtain quantum thermal properties. It begins with the textbook expression for the partition function

$$Q(T) = tr[e^{-\beta H}], \tag{5}$$

where H is the Hamiltonian operator. Evaluating this trace is computationally difficult except in relatively simple cases where eigenvalues of H are known or where the diagonal elements of the H-matrix can be efficiently obtained in a complete basis. For CH_5^+ neither of these is currently feasible. Feynman showed how his general path integral formulation of quantum mechanics can be used to evaluate Q(T) accurately using short (imaginary) time slicing.[28] The final result can be written as

$$Q(T) \approx tr[e^{-\beta H_n}], \tag{6}$$

$$H_P = \sum_{i=1}^{N}\sum_{j=1}^{P}(\frac{p_{i,j}^2}{2m_i} + \frac{1}{2}m_i\omega_P^2|\mathbf{x}_{i,j} - \mathbf{x}_{i,j+1}|^2) + \sum_{j=1}^{P} V(\mathbf{x}_{i,j}), \tag{7}$$

$$\mathbf{x}_{i,P+1} = \mathbf{x}_{i,1}, \omega_P = P/\beta\hbar. \tag{8}$$

where $\mathbf{x}_{i,P}$ represents the coordinates of each atom in the molecule/cluster etc. for the Pth replica and the trace is evaluated using the classical phase space averaging in the expanded space of a "ring polymer". In practice this averaging is done more efficiently using molecular

dynamics with the above Hamiltonian, augmented by an *ad hoc* thermostat. In the present case each CH_5^+ is replicated P times and each replica interacts with all other replicas via harmonic springs with frequency ω_P.

In the present work the new CH_5^+ PES was interfaced with the i-PI software[29] for performing classical and path integral molecular dynamics simulations (MD and PIMD). For classical MD simulations, one trajectory was propagated for 1 ns with time step of 0.5 fs for each temperature (10 K and 50 K). The Langevin thermostat was applied in the corresponding canonical ensemble (NVT). For PIMD simulations, the trajectory was also propagated for 1 ns with time step of 0.5 fs for each temperature (10 K and 50 K). A total number of 128 beads and 64 beads were used for the PIMD simulation with the PIGLET thermostat[30] at 10 K and 50 K respectively. For structural analysis of radial distribution functions, the first 250 ps of each trajectory was considered as equilibrium steps and the structures in the remaining 750 ps of the trajectory were analyzed.

Results and Discussion

Potential Energy Surface

In addition to comparing the PES energies to the calculated ones, we tested the potential energy surface in three additional ways. First, we determined the geometries of low-energy stationary points on the surface, locating the global minimum (C_s(I)), the lower saddle point (C_s(II)), and the upper saddle point (C_{2v}). These were then compared to the CCSD(T)/TZP2+f bond lengths[4] quoted in ref. 11. We found that the MAEs for the internuclear distances of the three structures were 0.15% for C_s(I), 0.50% for C_s(II) and 0.06% for C_{2v}; the geometries of the stationary points are given in the Supplementary Information. The global minimum structure is shown in Fig. 2

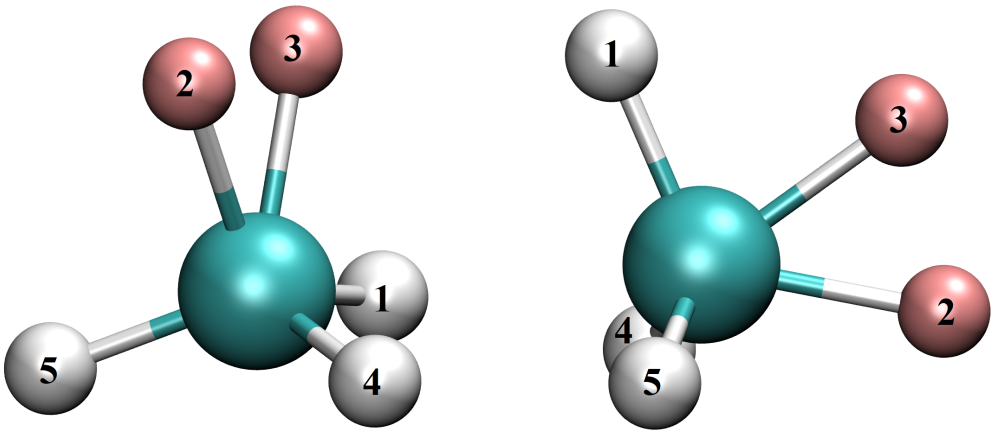

Figure 2: Minimum structure of CH_5^+ from two orientations. The diatomic fragment is indicated by H atoms 2 and 3. The two CH distances are the same for this fragment and are also the shortest ones. The cartesian coordinates of this structure and also two low-lying saddle points are given in the Supplementary Information.

Second, the energies of the saddle points on the PES, relative to the global minimum at C_s(I), were determined to be 32 cm^{-1} and 341 cm^{-1}, very similar to the CCSD(T) values, 37.7 cm^{-1} and 331.2 cm^{-1}.[11] and the CCSD(T)-R12 single-point energies of 35 and 280 cm^{-1}.[5]

Third, we determined the harmonic vibrational energies for the three stationary points and compared these to the CCSD(T) values. Briefly, the MAE for the frequencies of the C_s(I) global minimum was 5.15 cm^{-1}, that for the C_s(II) saddle point was 6.82 cm^{-1}, and that for C_{2v} saddle point was 7.05 cm^{-1}. The frequencies for the surface stationary points and the CCSD(T) stationary points are also provided in the Supplementary Information.

The close agreement of these tests with the benchmark values indicates that the surface quite accurately reproduces the structures, energies and Hessians of these three important structures.

DMC and PIMD Results

To begin we show in Figure 3 previous diffusion Monte Carlo (DMC) and molecular dynamics (MD) results for probability distributions for $CH_2D_3^+$ using the first CH_5^+ PES obtained

at the MP2/cc-pVTZ level of theory.[13] The DMC results are the standard ones with no constraints, i.e., no guiding function, and these pertain to the ground ro-vibrational state. The MD results are from standard microcanonical trajectories at total energy equal to the DMC zero-point energy (ZPE) of 9148 cm^{-1}. The most striking difference in these broad distributions is for CD vs CH, shown in panels (a) and (c). In the microcanonical MD simulations these are the same, implying complete scrambling of the H and D atoms. By contrast the quantum DMC distributions are different and show a strong preference for the $CD_3^+...H_2$ structure. The results in panels (b) and (d) are interesting for the total distribution, which are similar. However, the ones for the HH distance are different, as expected. The DMC results show a broad peak characteristic for the "diatomic" fragment, whereas the MD distribution has a broad maximum corresponding to the CH_3^+ fragment.

The localization of the H atoms to the HH fragment is clearly a quantum effect and can be rationalized using a simple harmonic analysis at the various possible arrangements of the atoms. The lowest harmonic zero-point energy is indeed the one indicated. Given the large anharmonicity of this cation this result may be fortuitous. Finally, note that the MP2-based PES has the two important low-lying saddle points with energies of 43 and 193 cm^{-1}. The higher energy one is significantly lower than the CCSD(T) one of 341 cm^{-1}. This difference should be kept in mind for readers who examine the new results below and these earlier ones and see some minor quantitative differences.

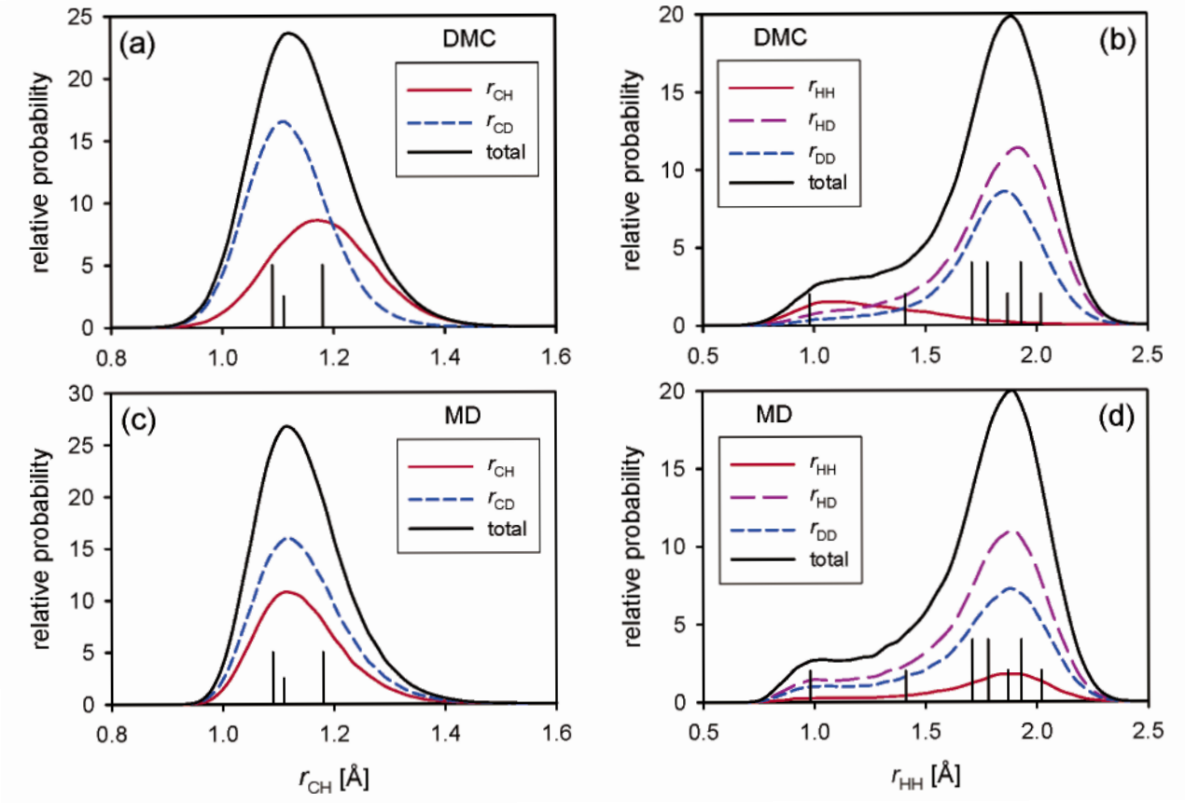

Figure 3: Distribution functions of CH, CD, HH and HD distances for $CH_2D_3^+$ from classical MD (blue) and DMC simulations. Distances at global minimum geometry are indicated in black sticks. Reprinted with permission from reference 13.

DMC results using the new PES are shown in Figure 4. These are smoothed histograms of the distribution of walkers and so these plots represent the zero-point wavefunction and not the probability. However, since the wavefunction is positive definite the results shown are certainly indicative of the structure of the molecule in the ground vibrational state. As such, the qualitative agreement with the DMC probability distributions shown above for the MP2 PES is both satisfying and not unexpected. In addition, inspection of the present DMC results with previous DMC wavefunction projections[31] using the CCSD(T)-based PES of Jin et al.[11] show good agreement. Next we present PIMD and MD results for CH_5^+ and $CH_2D_3^+$ at 10 and 50 K.

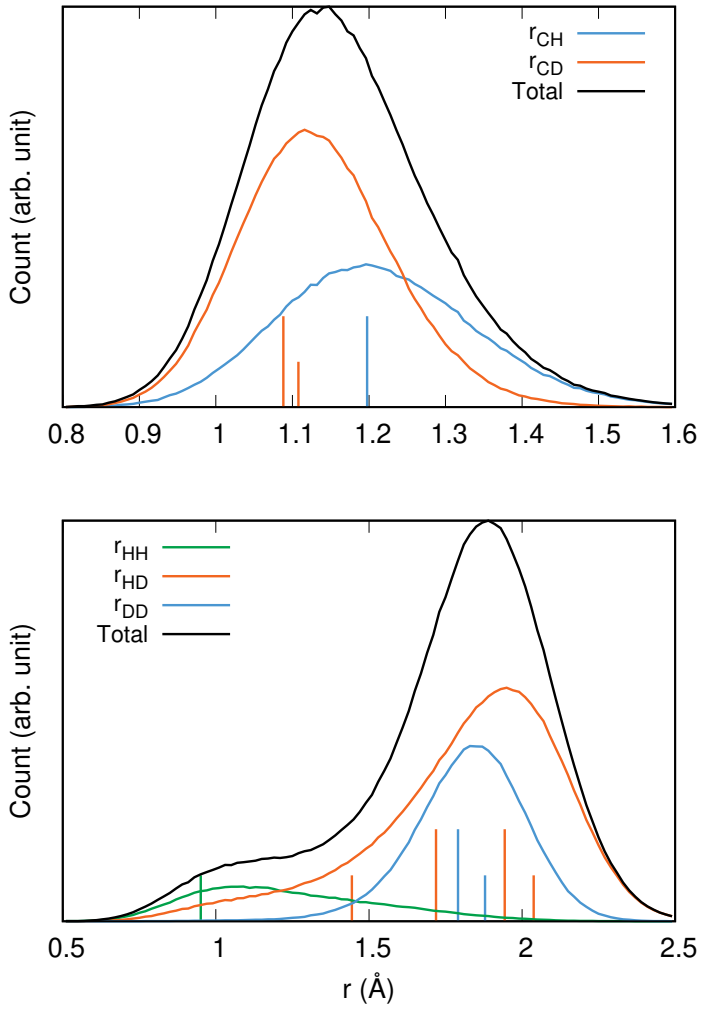

Figure 4: Projection of the ground-state wavefunction (obtained from DMC calculations) of $CH_2D_3^+$ onto CH/D distances (upper) and HH/DD distances (lower). Distances at the global minimum geometry are indicated in sticks.

PIMD

Distribution functions for CH_5^+ from canonical PIMD and MD calculations at 10 K are shown in Fig. 5. Note the latter are very different from the microcanonical ones shown in Fig. 3. At these low temperatures the expectation is that the canonical MD results sample configurations about the minimum and indeed that is seen. The PIMD distributions are broad, and in fact are quite similar to the earlier DMC distributions for CH_5^+,[31] using the CCSD(T)-based potential of Jin *et al.*[11] The similarity is also seen here for the sum of

the DMC CH and CD distributions and HH and HD/DD distributions shown in the figures above. This is not unexpected since the PIMD distributions should approach the DMC as the temperature approaches 0 K. Actually reaching 0 K in PIMD simulations is computational unfeasible as β goes to infinity in this limit.

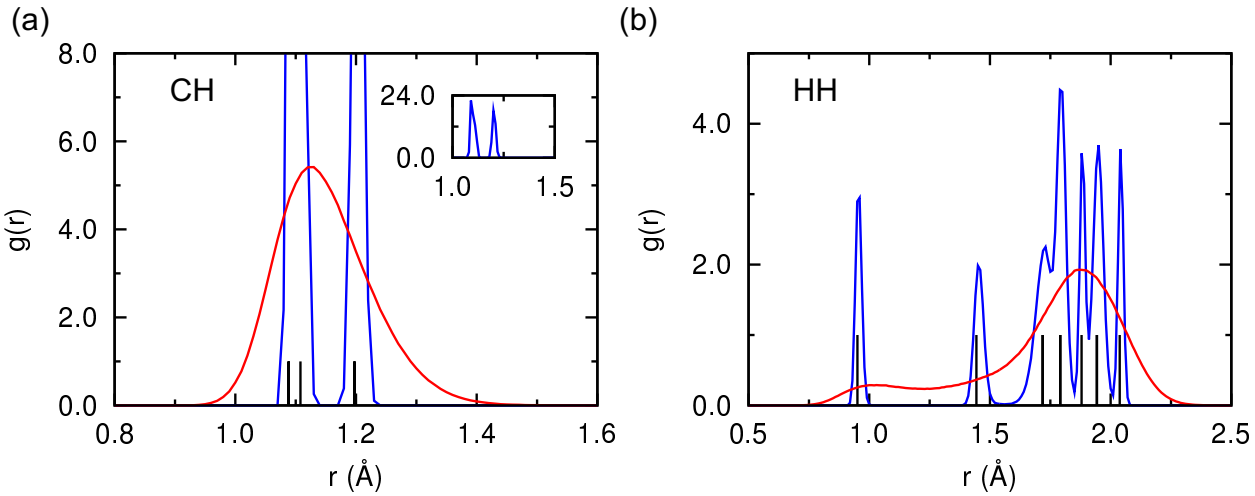

Figure 5: Distribution functions of CH and HH distances for CH_5^+ from classical MD (blue) and PIMD (red) simulations at 10 K. Distances at global minimum geometry are indicated in black sticks.

The PIMD distributions for CH_5^+ using the new PES at 10 and 50 K are shown in Figure 6. As seen, there is some broadening of the distribution at the higher temperature, as expected, but overall the distributions shown are quite similar.

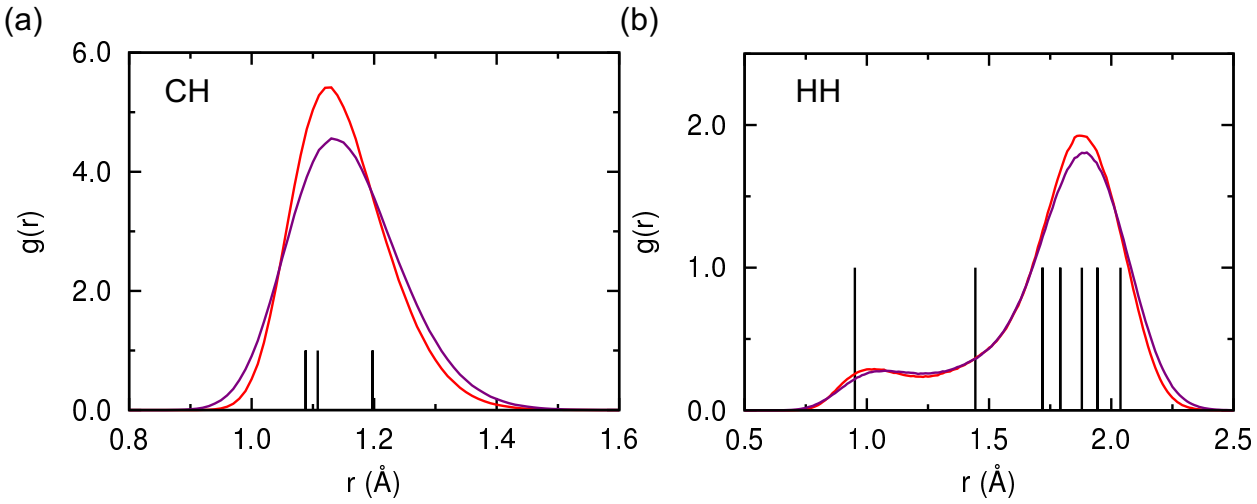

Figure 6: Distribution functions of CH and HH distances for CH_5^+ from PIMD simulations at 10 K (red) and 50K (purple). Distances at global minimum geometry are indicated in black sticks.

Next, we consider the canonical MD and PIMD distributions for $CH_2D_3^+$ at 10 K. These are shown in Figs. 7 and 8. Note that the initial conditions for these simulations are at the minimum with the two H atoms in the diatomic site. Starting the MD simulation in any other arrangement would not sample other arrangements at this low temperature. In principle the PIMD simulation would eventually relax to the diatomic HH arrangement; however, this could take a long time and so this was not done.

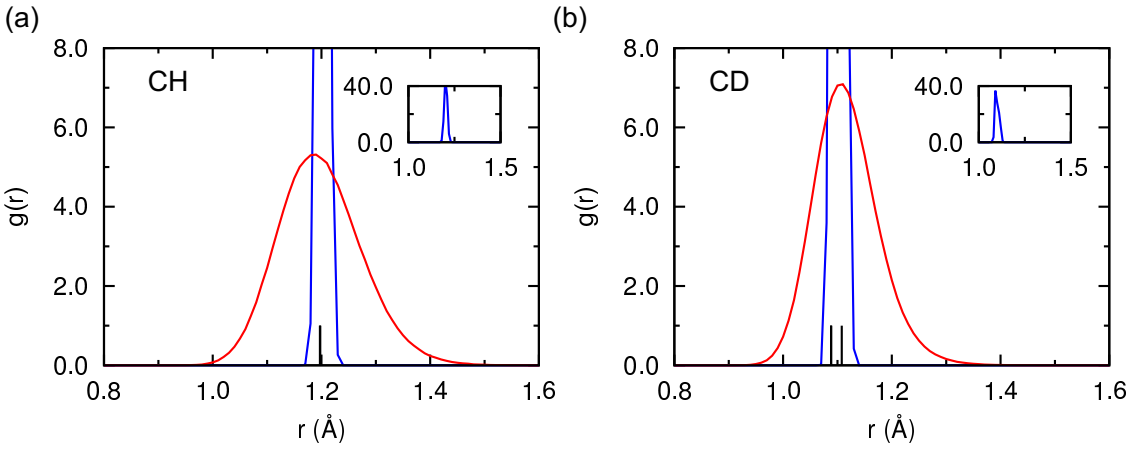

Figure 7: Distribution of CH and CD distances for $CH_2D_3^+$ from classical MD (blue) and PIMD (red) simulations at 10 K. Distances at minimum geometry with the H atoms in the diatomic site are indicated by black sticks.

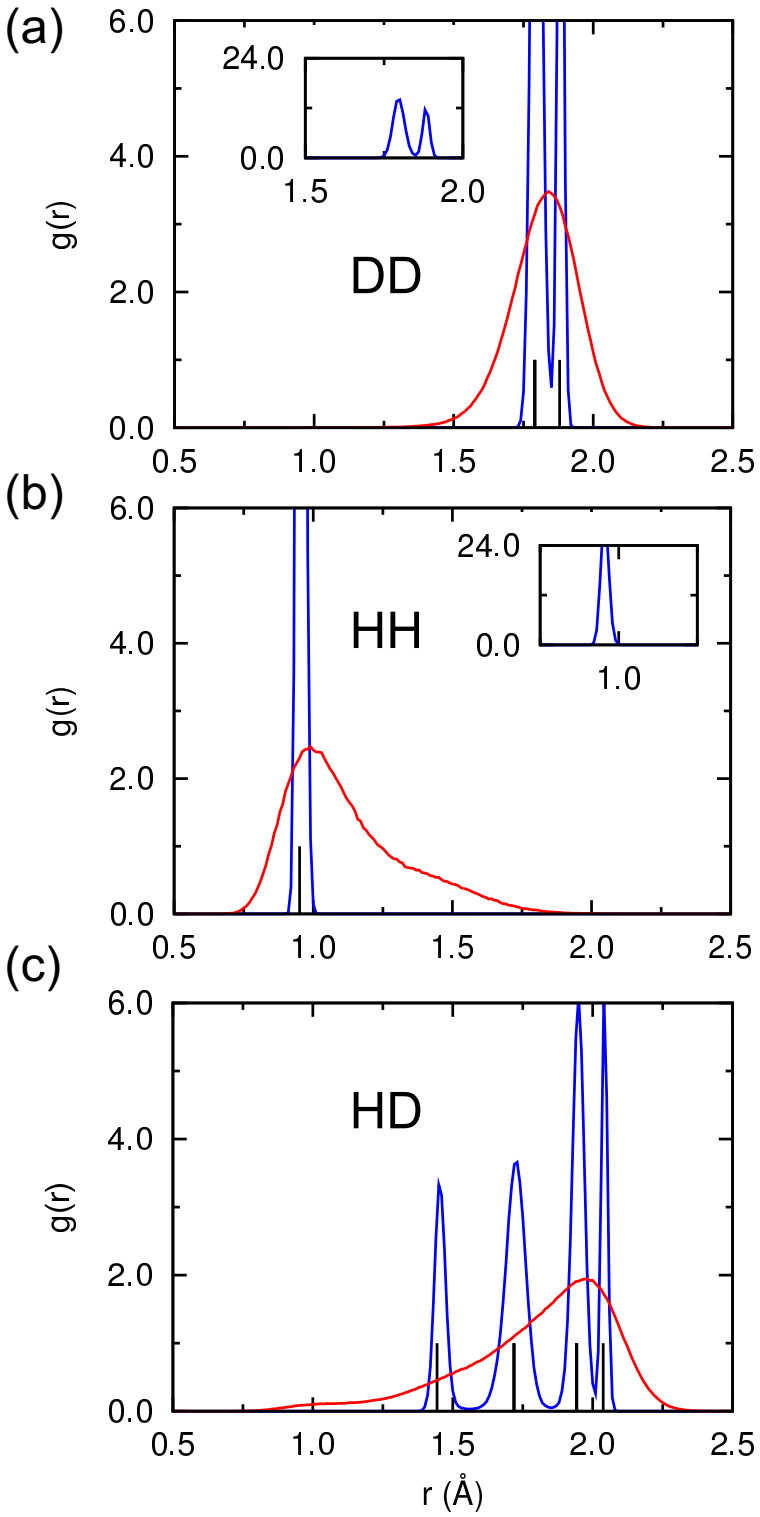

Figure 8: Distributions of DD, HH and HD distances for $CH_2D_3^+$ from classical MD (blue) and PIMD (red) simulations at 10 K. Distances at global minimum geometry are indicated by black sticks.

Finally, we examine the PIMD distributions for $CH_2D_3^+$ at 10 and 50 K in Figures 9 and 10. As seen in the former some broadening is seen. The results in the latter figure are more interesting. Namely, panel (b) of that figure shows an HH distribution at 50 K that is significantly different from the 10 K one. The distinct secondary maximum at 2 A is a clear indication of significant delocalization of the H atoms from the diatomic site and to the "CH_3^+" site where at that minimum the HH distribution shows a broad maximum at roughly 2 A, cf. Fig. 6. This result is a significant prediction of the present work, which hopefully will stimulate experimental investigation of the temperature dependence of the structure of $CH_2D_3^+$. Ivanov et al reported AIMD calculations for isotopologs of CH_5^+ including $CH_2D_3^+$ and performed PIMD calculations at 110 K in order to weight the classical IR spectrum.[32] They reported the following percentages of the number of H atoms in the diatomic fragment: 1 H 57%, 2H 35% and 0H 8%. This delocalization at 110 K is consistent with the results here which indicate an onset of delocalization at 50 K .

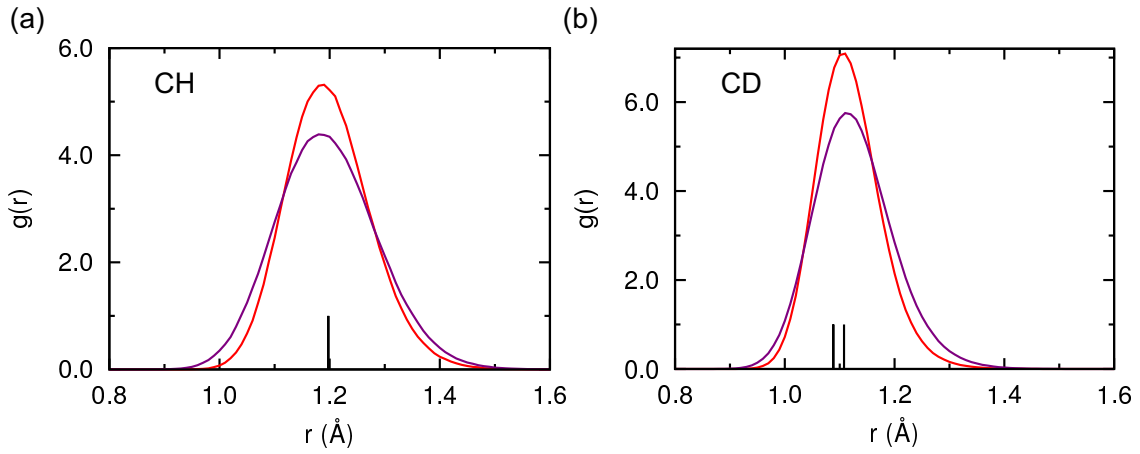

Figure 9: Distribution of CH and CD distances for $CH_2D_3^+$ from PIMD simulations at 10 K (red) and 50 K (purple). Distances at minimum geometry are indicated by black sticks.

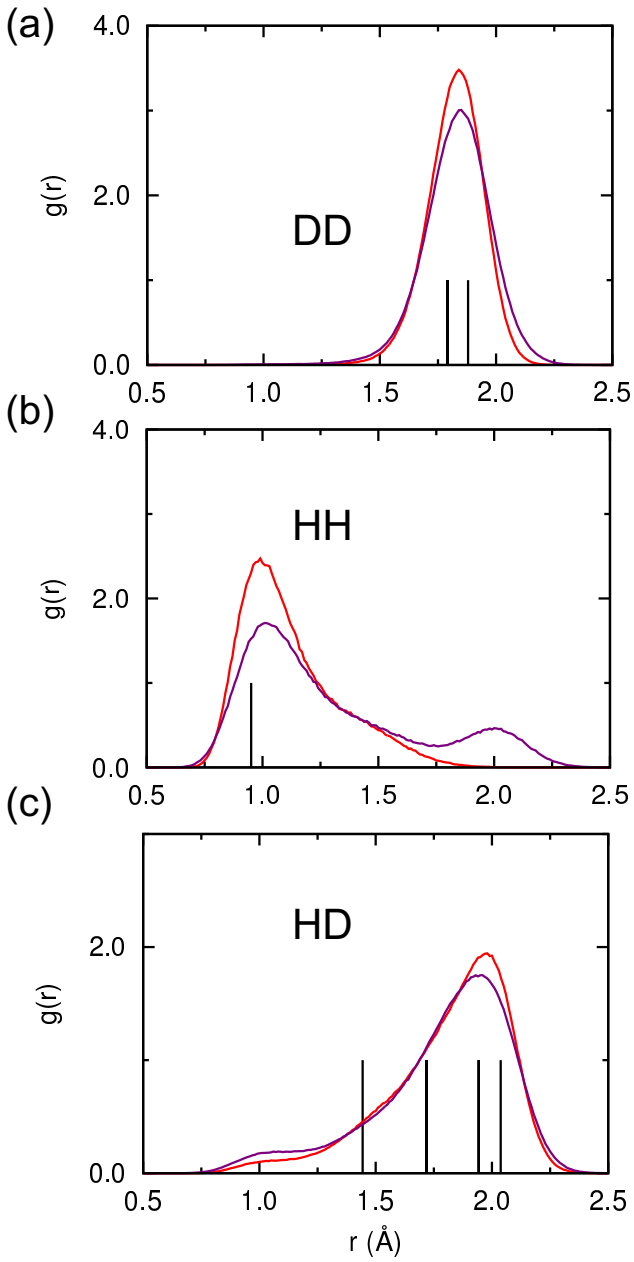

Figure 10: Distribution functions of DD, HD, and HH distances for $CH_2D_3^+$ from PIMD simulations at 10 K (red) and 50K (purple). Distances at global minimum geometry are indicated in black sticks.

Summary

We reported a new fit to previous CCSD(T)/aug-cc-pVTZ energies of CH_5^+ using our latest PIP software, which provides fast analytical gradients.[23] The new fit is precise and accurately

provides the geometry and energies of the critical two low-lying saddle points that govern the highly fluxional motion of this cation. Canonical PIMD and MD simulations at 10 and 50 K of the distributions of CH and HH distances of CH_5^+ were reported. Diffusion Monte Carlo and MD and PIMD calculations of the distribution of CH, CD, HH, DD, HD distances for $CH_2D_3^+$ were also reported. In this case the two H atoms prefer the diatomic site predominantly except at 50 K, where delocalization of these atom to the "CH_3^+" site is seen. Finally, we note that present calculations do not consider the nuclear spin statistics and future work doing so would be valuable.

Acknowledgment

We dedicate this paper to the memory of Timothy Lee. JMB and PP acknowledge support from NASA grant 80NSSC20K0360.

References

(1) White, E. T.; Tang, J.; Oka, T. CH_5^+: The Infrared Spectrum Observed. *Science* **1999**, *284*, 135–137.

(2) Oka, T. Taming CH_5^+, The Enfant Terrible of Chemical Structures. *Science* **2015**, *347*, 1313–1314.

(3) Olah, G. A. My Search for Carbocations and Their Role in Chemistry (Nobel Lecture). *Angew. Chem. Int. Ed. Engl.* **1995**, *34*, 1393–1405.

(4) Schreiner, P. R.; Kim, S. J.; Schaefer, H. F.; Schleyer, P. v. R. CH_5^+: The Never-Ending Story or the Final Word? *J. Chem. Phys.* **1993**, *99*, 3716.

(5) Müller, H.; Kutzelnigg, W.; Noga, J.; Klopper, W. CH_5^+: The Story Goes on. An Explicitly Correlated Coupled-Cluster Study. *J. Chem. Phys.* **1997**, *106*, 1863–1869.

(6) Marx, D.; Parrinello, M. CH_5^+: The Cheshire Cat Smiles. *Science* **1999**, *284*, 59–61.

(7) Brown, A.; Braams, B. J.; Christoffel, K.; Jin, Z.; Bowman, J. M. Classical and Quasiclassical Spectral Analysis of CH_5^+ Using an *Ab Initio* Potential Energy Surface. *J. Chem. Phys.* **2003**, *119*, 8790–8793.

(8) Brown, A.; McCoy, A. B.; Braams, B. J.; Jin, Z.; Bowman, J. M. Quantum and Classical Studies of Vibrational Motion of CH_5^+ on a Global Potential Energy Surface Obtained from a Novel *Ab Initio* Direct Dynamics Approach. *J. Chem. Phys.* **2004**, *121*, 4105–4116.

(9) McCoy, A. B.; Braams, B. J.; Brown, A.; Huang, X.; Jin, Z.; Bowman, J. M. *Ab Initio* Diffusion Monte Carlo Calculations of the Quantum Behavior of CH_5^+ in Full Dimensionality. *J. Phys. Chem. A* **2004**, *108*, 4991–4994.

(10) Thompson, K. C.; Crittenden, D. L.; Jordan, M. J. T. CH_5^+: Chemistry's Chameleon Unmasked. *J. Amer. Chem. Soc.* **2005**, *127*, 4954–4958.

(11) Jin, Z.; Braams, B. J.; Bowman, J. M. An *Ab Initio* Based Global Potential Energy Surface Describing $CH_5^+ \rightarrow CH_3^+ + H_2$. *J. Phys. Chem. A* **2006**, *110*, 1569–1574.

(12) Mann, J. E.; Xie, Z.; Savee, J. D.; Braams, B. J.; Bowman, J. M.; Continetti, R. E. Probing the Structure of CH_5^+ by Dissociative Charge Exchange. *J. Amer. Chem. Soc.* **2008**, *130*, 3730–3731.

(13) McCoy, A. B.; Braams, B. J.; Brown, A.; Huang, X.; Jin, Z.; Bowman, J. M. *Ab Initio* Diffusion Monte Carlo Calculations of the Quantum Behavior of CH_5^+ in Full Dimensionality. *J. Phys. Chem. A* **2004**, *108*, 4991.

(14) Huang, X.; Johnson, L. M.; Bowman, J. M.; McCoy, A. B. Deuteration Effects on the Structure and Infrared Spectrum of CH_5^+. *J. Amer. Chem. Soc.* **2006**, *128*, 3478–3479.

(15) Huang, X.; McCoy, A. B.; Bowman, J. M.; Johnson, L. M.; Savage, C.; Dong, F.; Nesbitt, D. J. Quantum Deconstruction of the Infrared Spectrum of CH_5^+. *Science* **2006**, *311*, 60–63.

(16) Deskevich, M. P.; McCoy, A. B.; Hutson, J. M.; Nesbitt, D. J. Large-amplitude quantum mechanics in polyatomic hydrides. II. A particle-on-a-sphere model for XHn(n=4,5). *J. Chem. Phys.* **2008**, *128*, 094306.

(17) Wang, X.-G.; Carrington, T. Calculated Rotation-Bending Energy Levels of CH_5^+ and a Comparison with Experiment. *J. Chem. Phys* **2016**, *144*, 204304.

(18) Fábri, C.; Quack, M.; Császár, A. G. On the Use of Nonrigid-Molecular Symmetry in Nuclear Motion Computations Employing a Discrete Variable Representation: A Case Study of the Bending Energy Levels of CH_5^+. *J. Chem. Phys.* **2017**, *147*, 134101.

(19) Simkó, I.; Fábri, C.; Császár, A. G. Quantum-Chemical and Quantum-Graph Models of the Dynamical Structure of CH_5^+. *J. Comput. Theor. Chem.* **2023**, *19*, 42–50.

(20) Brown, A.; Braams, B. J.; Christoffel, K.; Jin, Z.; Bowman, J. M. Classical and Quasiclassical Spectral Analysis of CH_5^+ Using an *Ab Initio* Potential Energy Surface. *J. Chem. Phys.* **2003**, *119*, 8790–8793.

(21) Nandi, A.; Qu, C.; Bowman, J. M. Using Gradients in Permutationally Invariant Polynomial Potential Fitting: A Demonstration for CH_4 Using as Few as 100 Configurations. *J. Chem. Theor. Comp.* **2019**, *15*, 2826–2835.

(22) Houston, P. L.; Qu, C.; Nandi, A.; Conte, R.; Yu, Q.; Bowman, J. M. Permutationally Invariant Polynomial Regression for Energies and Gradients, Using Reverse Differentiation, Achieves Orders of Magnitude Speed-Up with High Precision Compared to Other Machine Learning Methods. *J. Chem. Phys.* **2022**, *156*, 044120.

(23) Houston, P. L.; Qu, C.; Yu, Q.; Conte, R.; Nandi, A.; Li, J. K.; Bowman, J. M. PESPIP: Software to Fit Complex Molecular and Many-Body Potential Energy Surfaces with Permutationally Invariant Polynomials. *J. Chem. Phys.* **2023**, *158*, 044109.

(24) Anderson, J. B. A Random-Walk Simulation of the Schrödinger Equation: H_3^+. *J. Chem. Phys.* **1975**, *63*, 1499–1503.

(25) Suhm, M. A.; Watts, R. O. Quantum Monte Carlo Studies of Vibrational States in Molecules and Clusters. *Phys. Rep.* **1991**, *204*, 293–329.

(26) McCoy, A. B. Diffusion Monte Carlo Approaches for Investigating the Structure and Vibrational Spectra of Fluxional Systems. *Int. Rev. Phys. Chem.* **2006**, *25*, 77–107.

(27) Kosztin, I.; Faber, B.; Schulten, K. Introduction to the Diffusion Monte Carlo Method. *Am. J. Phys.* **1996**, *64*, 633–644.

(28) Feynman, R. P.; Hibbs, A. R. *Quantum Mechanics and Path Integrals*; McGraw-Hill: New York, 1965.

(29) Kapil, V. et al. i-PI 2.0: A Universal Force Engine for Advanced Molecular Simulations. *Comput. Phys. Commun.* **2019**, *236*, 214–223.

(30) Ceriotti, M.; Manolopoulos, D. E. Efficient First-Principles Calculation of the Quantum Kinetic Energy and Momentum Distribution of Nuclei. *Phys. Rev. Lett.* **2012**, *109*, 100604.

(31) Johnson, L. M.; McCoy, A. B. Evolution of Structure in CH_5^+ and Its Deuterated Analogues. *J. Phys. Chem. A* **2006**, *110*, 8213–8220.

(32) Ivanov, S.; Asvany, O.; Witt, A.; Hugo, E.; Mathias, G.; Redlich, B.; Marx, D.; Schlemmer, S. Quantum-Induced Symmetry Breaking Explains Infrared Spectra of CH_5^+ Isotopologues. *Nat. Chem.* **2010**, *2*, 298–302.